# Utility of Ground-penetrating Radar in Near-surface, High-resolution Imaging of Lansing-Kansas City (Pennsylvanian) Limestone Reservoir Analogs

Alex Martinez[1], Joseph M. Kruger[2], and Evan K. Franseen[1]
[1]Kansas Geological Survey, 1930 Constant Ave., Lawrence, KS 66047
[2]Idaho State University, Department of Geology, Pocatello, ID 83209-8072

## Abstract

High-resolution ground-penetrating radar (GPR) is a subsurface imaging tool that can extend results gained from studies of reservoir-analog outcrops and add detailed information about reservoir analogs that is unavailable from either seismic data or well control alone. Integration of GPR-reflection information and outcrop photomosaics allowed detailed study of subtle changes in lithology and bedding surfaces by comparing lateral and vertical changes in GPR-reflection character with outcrop features. Outcrops are valuable for confirming interpretations of reflections and providing velocity information for the GPR data. Outcrops of two Lansing-Kansas City Group limestone units, the Captain Creek Limestone and the Plattsburg Limestone, were used as test sites to determine the vertical imaging resolution, penetration depth, and reflection character of high-frequency (500 MHz) GPR in interbedded carbonate and shale units, where the carbonate units contained thin interbeds of shale. Features as small as 0.1–0.2 m (0.3–0.7 ft)—including major architectural elements (such as major and minor bounding surfaces) and internal features (such as fractures, internal bedding, and crossbedding)—were successfully imaged and confirmed by outcrop data. Variations in GPR-reflection character between geologic units allowed recognition of argillaceous limestone units in the subsurface. Although shale and soil at the surface generally impeded GPR signal penetration, thin shale layers and shale at bounding surfaces actually enhanced reflectivity and aided in interpretation. Our results indicate that GPR can be successfully used as an aid in outcrop studies to provide quantitative data for use in reservoir modeling.

Pennsylvanian, cyclothemic, carbonate strata that crop out in northeastern Kansas are direct analogs for stratal units that are petroleum reservoirs in central and western Kansas. Although the reservoirs have been successfully produced for many years, they still contain significant accumulations of hydrocarbons. New methods are being sought to identify thinner zones and better understand reservoir architecture at increasingly finer scales. Many of the reservoirs have multiple pay zones within the complex reservoir heterogeneity that are affected by poorly understood facies changes, stratal geometries, diagenesis, and interbedded shales and sandstones that provide seals to reservoir facies (Newell et al., 1987).

Outcrop studies of reservoir analogs can provide important insights into complex reservoir architecture. Increasingly, outcrop studies of Pennsylvanian strata in Kansas integrate modern concepts of sequence stratigraphy (e.g., Watney et al., 1989; Feldman and Franseen, 1991) with other methods, such as high-resolution seismic data (Miller et al., 1995; Franseen et al., 1995), in order to better understand geometries, facies patterns, and diagenetic trends, not only at the cyclothem scale, but also of strata within individual cyclothems. Such studies, focusing on higher resolution, can aid in better understanding reservoir architecture and controls, especially in smaller-scale reservoirs where general patterns of stratal geometries, thicknesses, and diagenetic trends, which do not correlate with structure, are important in controlling reservoir development (e.g., Brown, 1963; Watney, 1980).

Seismic-reflection data provide general information about subsurface structures and usually image features greater than 10–15 m (33–49 ft) in thickness. Well data, on the other hand, provide very detailed information about the area immediately around the well. Outcrop-analog studies are an important facet of reservoir studies because they bridge the gap in resolution between seismic and well information and allow detection of small-scale lateral variations of detailed stratigraphic architecture, which can affect oil recovery and may be missed by using only seismic or well data.

Ground-penetrating radar (GPR) is a near-surface, nonintrusive geophysical technique similar to seismic reflection that images the subsurface at a much higher resolution (Pratt and Miall, 1993; Gawthorpe et al., 1993; Liner and Liner, 1995; Beres et al., 1995; Bridge et al., 1995; Jol et al., 1996; Martinez et al., 1996). In addition to the high-

resolution imaging, GPR is a potentially useful method in outcrop studies because it can provide stratal information in poorly exposed areas and three-dimensional stratal characteristics beyond the outcrop face (e.g., Beaty et al., 1997). Because GPR profiles are usually gathered as common offset data, minimal digital-signal processing is involved when compared to shallow seismic-reflection methods. Data collection is rapid and non-invasive, allowing profiles to be collected easily and quickly without altering a study site. The digital data collected are easily manageable on computer workstations with software developed for the petroleum industry to interpret seismic data. Collection of multiple profiles or three-dimensional grids of GPR data at study sites allows outcrop studies to be extended into the third-dimension, sometimes greatly enhancing understanding of stratigraphic architecture (Beaty et al., 1997). Grids of GPR data can also be used to supplement and connect discrete core information.

Typical GPR frequencies for stratigraphic studies range from 10 to 100 MHz, resulting in vertical imaging resolutions of 1.5–1.0 m (4.9–3.3 ft) (Beres et al., 1995; Bridge et al., 1995; Dominic et al., 1995). Although such resolution is sufficient for targets that are relatively large or laterally extensive, it may be insufficient for imaging detailed stratigraphy needed for some reservoir studies. Use of higher-frequency antennas (e.g., greater than 200 MHz) increases resolution enough to image fine-scale stratigraphic variations, but penetration depths decrease due to signal attenuation, which increases with frequency (Davis and Annan, 1989).

The purpose of our study was to determine the usefulness and limitations of GPR as an additional tool in characterizing Pennsylvanian, carbonate, reservoir-analog outcrops at a high resolution. To date, only a few studies have examined the usefulness of GPR as a stratigraphic tool in carbonate strata (Pratt and Miall, 1993; Liner and Liner, 1995). These studies focused on thick, relatively homogeneous carbonate packages. Our study differs in that we imaged interbedded carbonate and shale strata (0.2–5 m; 0.7–16.4 ft), and the carbonate beds variously contained thin (less than 0.01 m; 0.03 ft) shale layers.

The study outcrops were divided into several different units based upon GPR reflections and stratigraphy. The interpreted data show excellent correlation between stratigraphic surfaces seen on the outcrop face and those imaged via high-frequency GPR. In this study GPR imaged subsurface features as thin as 0.1–0.2 m (0.3–0.7 ft). However, data quality was severely diminished in some areas by significant signal attenuation, which was caused by either shales or clay-rich soils at the surface. The results of our study indicate that GPR is a useful method for imaging and adding to outcrop studies of carbonate-reservoir analogs. Our study also provides information on the limitations of GPR in the study of cyclic strata composed of interbedded carbonate and siliciclastic strata and gives direction for future studies.

# GPR Data Acquisition and Processing

## General Methods

GPR acquisition, processing, and display are very similar to the methods used in seismic reflection. However, GPR has much higher resolution and is sensitive to changes in electromagnetic, rather than acoustic, properties. GPR reflections are caused by electromagnetic waves encountering media that have different electrical properties—namely, boundaries consisting of dielectric-constant contrasts. Reflection strength is approximately proportional to the difference of the dielectric constants at the boundary (Davis and Annan, 1989). Values for dielectric constants range from 1 for air, 4 to 8 for limestone, 5 to 13 for shale, 5 to 40 for clay, and 81 for water (Daniels, 1996; Davis and Annan, 1989; Schon, 1996). Dielectric-constant values affect the velocity of electromagnetic waves through a material. One-way velocities for the following materials are 0.3 m (1 ft)/nanosecond (ns) for air, 0.11–0.15 m (0.36–0.49 ft)/ns for limestone, 0.08–0.13 m (0.26–0.43 ft)/ns for shale, 0.05–0.13 m (0.16–0.43 ft)/ns for clay, and 0.03 m (0.09 ft)/ns for water. Antenna frequencies typically range from 10 to 1,000 MHz. Vertical resolution varies from 1 to 1.5 m (3.3–4.9 ft) for low-frequency antennas (10–100 MHz) to 0.02 to 0.3 m (0.06–0.98 ft) for higher-frequency antennas (500–1,000 MHz) for most materials (Davis and Annan, 1989). These reported velocities were used as a basis for elevation corrections and interpretation in this study and were verified by comparison of reflection times with unit thicknesses on the outcrop.

GPR data are typically shown as common offset profiles with trace-amplitude variations representing differences in reflectivity. The vertical scale of a profile shows two-way travel-time, usually in nanoseconds ($ns = 1 \times 10^{-9}$ s), and the lateral scale is distance (trace spacing × number of traces) along the profile.

## Acquisition Parameters and Data Processing

Two study sites were chosen, based on the quality of exposure, ease of access, availability of geologic data from previous studies, and relevance of the facies and stratal geometries to reservoirs in Kansas. Site preparation included clearing the antenna path of obstructions, flagging the stations, collecting relative elevation information, and creating photomosaics of the outcrops for comparison with GPR data. The removal of material such as small rocks and grass from the antenna pathway enhanced antenna coupling with the ground and reduced spurious diffractions. It also allowed relatively consistent lateral antenna movement, ensuring even trace spacing. In order to retain the same antenna pathway for each of the profiles collected and to allow for the comparison of GPR data with the outcrop, stations were flagged at 1.5- or 3.1-m (4.9- or 10.2-ft) intervals. The antenna pathways

were located approximately 1 m (3.3 ft) behind the outcrop face to minimize the possibility of interference from out-of-plane reflections from the contact between rock and air. The collection of relative elevation information allowed the GPR data to be corrected for elevation differences. These corrections aided interpretation of reflections and correlation with the appropriate horizons on the outcrop. Elevations were obtained using a level and rod and are accurate to within 3 cm (1.2 in). The photomosaics were gathered in increments of either 7.6 or 15.2 m (24.9 or 49.8 ft), depending on the overall size of the outcrop at each site.

The equipment used for the study was a GSSI SIR System-8 GPR unit with a 500-MHz antenna. Record lengths of 20–80 ns were collected at a rate of 12.8 scans/second as the antenna was pulled along the pathway. For long profiles, greater than 30 m (98 ft) in length, the equipment was placed within a large-wheeled garden cart to facilitate continuous profiling. A short marker-pulse was recorded at each station, every 1.5 or 3.1 m (4.9 or 10.2 ft), and a double pulse was recorded at every fifth station, every 7.6 or 15.2 m (24.9 or 49.9 ft), in order to allow GPR data to be correlated with the outcrop. The tape unit recorded coherent, cable-induced system noise beginning at approximately 40 ns on each trace. This system noise masked some reflection information below this level, greatly reducing the signal-to-noise ratio of longer scans. System noise is readily identified because it always appears at the same times across the entire GPR record and has relatively consistent amplitude. Reflections differ in that they almost always have some variability in return times and change in amplitudes due to minor changes in velocities and depth to reflectors across an outcrop.

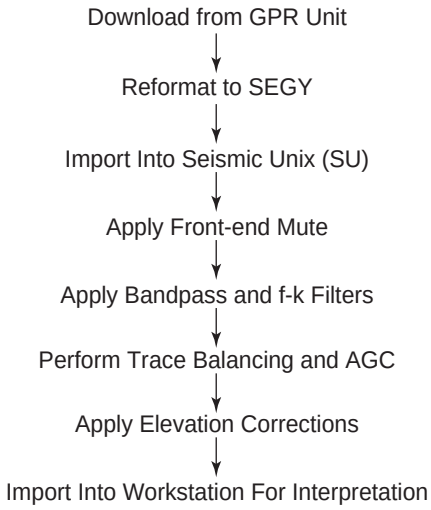


FIGURE 1. Generalized flow chart of GPR-data processing. Front-end mutes removed the high-amplitude reflection from the air-ground interface, allowing trace balancing to enhance low-amplitude reflection information. Frequency–wave number (f-k) filtering removed most of the system noise recorded below 40 ns. Low-frequency noise was removed or reduced by bandpass filters. Automatic gain controls (AGC) were used to allow low-amplitude events to become more visible and aid interpretation. Static shifts were applied to individual traces to account for elevation differences during data collection.

It was not possible to obtain velocity information from common-depth-point (CDP) gathers in this study because a monostatic antenna was used (e.g., the source and receiver were the same antenna). Instead, velocity information was obtained by comparing reflection travel times with interpreted unit thickness measured from the outcrop. Use of a bistatic antenna would allow CDP-velocity information to be gathered because the source and receiver antennas could be separated and data could be gathered at a variety of offsets. The GPR data for this study were collected in a continuous manner, which resulted in rapid data collection at the cost of lateral variability between traces and no vertical stacking. Collection of the data in a stepped manner would have allowed for even trace spacing as well as the vertical stacking of traces. Vertical stacking can increase signal-to-noise ratios of data and allow deeper reflectors to be imaged. Even spacings and vertical stacking of traces were not possible due to equipment limitations.

The GPR data were converted from RADAN format into 4-byte SEGY format for digital-signal processing with the program Seismic UNIX (SU). The data were time- and distance-scaled by a factor of $1 \times 10^6$ for viewing and processing purposes. Data processing did not vary much between the data from the two sites; a generalized processing flow chart is shown in fig. 1.

# GPR Data and Interpretations at the Study Sites

## Captain Creek Limestone Member

### Geologic Setting

The Captain Creek study site[1] (fig. 2) is located in northwestern Johnson County, Kansas (SQE-1 of Cunningham and Franseen, 1992). Two 106-m (348-ft) profiles of GPR data were collected to image features associated with the Captain Creek Limestone Member of the Stanton Limestone (within the Stanton depositional sequence of Watney et al., 1989) and the underlying Vilas Shale (which caps the subjacent Plattsburg depositional

[1] Recent studies and observations by one of the authors (Franseen) bring to question whether the strata at this study site belong to the Captain Creek Limestone and the Vilas Shale. However, these designations will be adhered to in this report as they have no bearing on the results of the outcrop and GPR study.

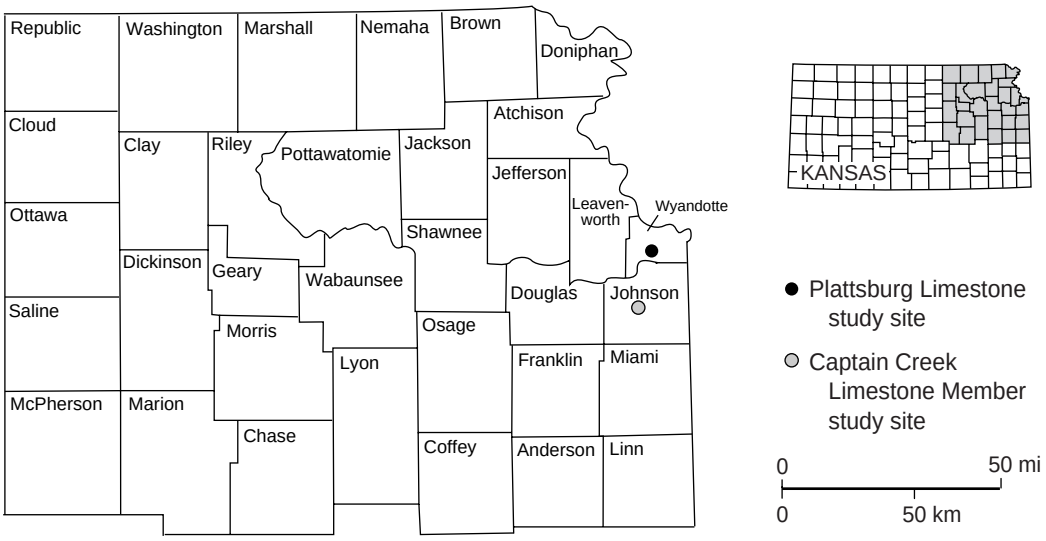


FIGURE 2. Map of eastern Kansas showing the locations of the outcrops used for this study.

sequence of Watney et al., 1989) (fig. 3). The site was chosen to determine the capabilities of GPR to image (1) the erosional contact between the Captain Creek and Vilas Shale; (2) the contact between the lower and upper Captain Creek submembers; and (3) internal bedding geometries and truncations in the lower and upper Captain Creek submembers.

The Vilas Shale is a gray mudstone, silty or sandy shale, or fine-grained sandstone containing mica and carbonized plant fragments (Cunningham and Franseen, 1992). It represents deltaic sedimentation during a relative lowstand in base level, and the upper surface is considered the sequence boundary of the Plattsburg depositional sequence (Watney et al., 1989).

The Captain Creek is the flooding unit within the Stanton depositional sequence and represents initial carbonate sedimentation during a relative rise in sea level (Watney et al., 1989). Cunningham and Franseen (1992) proposed two submembers for the Captain Creek Member. The lower submember is a gray or brown, conglomeratic lime grainstone composed of small, pebble-sized limestone clasts, bioclasts, and shale clasts and locally containing 0.1–0.3-m (0.3–0.9-ft)-scale horizontal bedding and local foresets. The upper Captain Creek submember is more massively bedded and typically occurs as a gray to light-brown phylloid, brachiopod, crinoid, and bryozoan lime wackestone-packstone.

The contact of the lower Captain Creek conglomeratic submember with the Vilas Shale indicates some erosional modification and is interpreted as a sequence boundary resulting from a relative sea-level fall. According to Cunningham and Franseen (1992), the Captain Creek conglomerates were deposited as tidal channel-fills in bathymetrically constricted areas between the Bonner Springs and Olathe algal mounds during a relative sea-level rise.

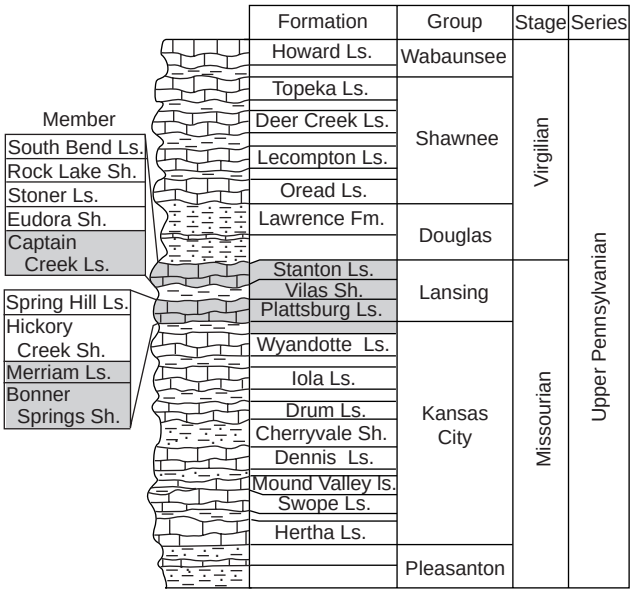


FIGURE 3. Stratigraphic column of Upper Pennsylvanian stata in northeastern Kansas. The two units used for this study, the Captain Creek Limestone Member and the Plattsburg Limestone, are highlighted.

## GPR Interpretation and Results

A map of the study site is shown in fig. 4. Figures 5 and 6 show uninterpreted and interpreted photomosaics and GPR data. The top of the roadcut where the GPR profiles were gathered has a rough, rocky terrain on either end and a thick overburden in the middle. The overburden thickness ranges from 0 to 1 m (3.3 ft), consists of a fine, silty soil (with approximately 45% clay, 40% silt, and 15%

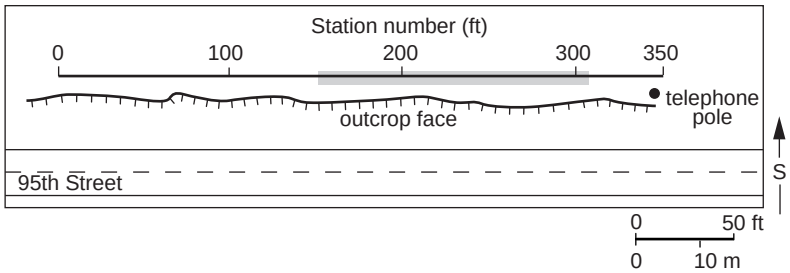


FIGURE 4. Map of the Captain Creek Limestone Member study site (see fig. 1 for location).

sand), and contains small fragments of chert and limestone. The clay-rich soil cover attenuated the signal greatly, resulting in no discernible reflection energy between stations 50 and 150. The thickening soil as observed on the outcrop (fig. 5) also caused a velocity pull-down in the reflection of up to 5 ns between stations 40 and 190 due to the change in velocity between the slower clay-rich overburden and the faster limestone (fig. 6). Minor variations in soil thickness, velocity, and topography resulted in short-period static shifts of 1 to 2 ns on GPR profiles. Some of this shifting may also have been due to intersecting hyperbolic diffractions from open or soil-filled fractures near the surface or to irregularities in bedding surfaces within the limestone. Changes in relative elevation did not appear to have any effect on limestone velocity. No out-of-plane reflections from the outcrop face were readily identifiable because profiles were taken far enough back from the outcrop face (approximately 1 m; 3.3 ft).

Relatively high amplitude reflections, which correlated with major outcrop stratigraphic divisions, are indicated by heavy dashed lines on figs. 5 and 6. The correlations were performed by comparing the outcrop photomosaics (and the outcrops themselves) with the GPR reflections. The major stratigraphic divisions were interpreted as the top of the upper Captain Creek submember (UC1), the top of the lower Captain Creek submember (LC1), and the top of the Vilas Shale (VS1). Reflections correlated with outcrop features between major unit divisions are identified by thin dashed lines.

*Upper Captain Creek Limestone Submember (UC1).*—The top of the upper Captain Creek submember (UC1) was indicated by a prominent reflection between stations 155 and 200 (fig. 6). Material above this reflector is primarily soil, which may have been created from the overlying Eudora Shale. On the outcrop the limestone layer does not sag (it is relatively horizontal), but on the GPR data there was a definite increase in the travel-time to the interpreted reflections from the limestone events. This is evidence that the observed velocity pull-downs were caused by thickening soil. Additionally, only when fractures were soil filled did they cause a velocity pull-down.

Soil-filled fractures near the top of the limestone caused weak diffractions and the interruption of continuity in the reflection near stations 185 and 190. Other evidence of fracturing included a velocity pull-down of reflections at station 190 and dipping events in the lower half of the submember between stations 195 and 210 adjacent to an isolated block between stations 200 and 205 (fig. 6). This may also be the cause of a prominent diffraction near the surface in the upper Captain Creek Limestone Member between stations 210 and 215. Several horizontal to low-angle dipping limestone layers in the upper Captain Creek submember are clearly visible and laterally traceable until they intersect the modern erosional surface between stations 190 and 250 (fig. 6).

*Lower Captain Creek Limestone (LC1).*—The contact between the lower and upper Captain Creek submembers (LC1), a 0.25-m (0.82-ft)-thick sandy shale, is visible between stations 180 and 275 (figs. 5 and 6). Internal bedding geometries within the lower Captain Creek were also imaged by GPR (fig. 6). Local convergent and divergent bedding geometries, and some truncations of beds likely associated with crossbedding at the base of the upper Captain Creek, were imaged between stations 240 and 285. Crossbed foresets were imaged by GPR in the lower half of the lower Captain Creek between stations 240 and 255. These crossbeds appeared to terminate against a relatively flat-lying bed above (fig. 6). Bed thinning is apparent on the outcrop west of station 270 and was visible on the GPR data as a decrease in time between reflections or a termination of reflections.

*Vilas Shale (VS1).*—The contact of the Captain Creek and Vilas Shale (VS1) was visible on the GPR data between stations 235 and 300 (figs. 5 and 6). The strength of this reflection was probably due to the large dielectric-constant contrast between limestone and shale. This contact was not imaged by GPR east of station 240 because of signal attenuation caused by increasing soil thickness on the top of the outcrop. Truncation of some beds within the Vilas Shale that are visible on the outcrop was not clearly imaged by GPR, probably because of its attenuating nature. As with the lower Captain Creek Limestone Member above it, the Vilas Shale appears to be slightly upwarped west of station 265 (fig. 5). However, the reflection associated with the top of the shale was subject to the same velocity effects as the overlying limestone, which may add to some of the apparent warping on the GPR data. Some evidence for true structural disruption of the shale came from a diffraction emanating

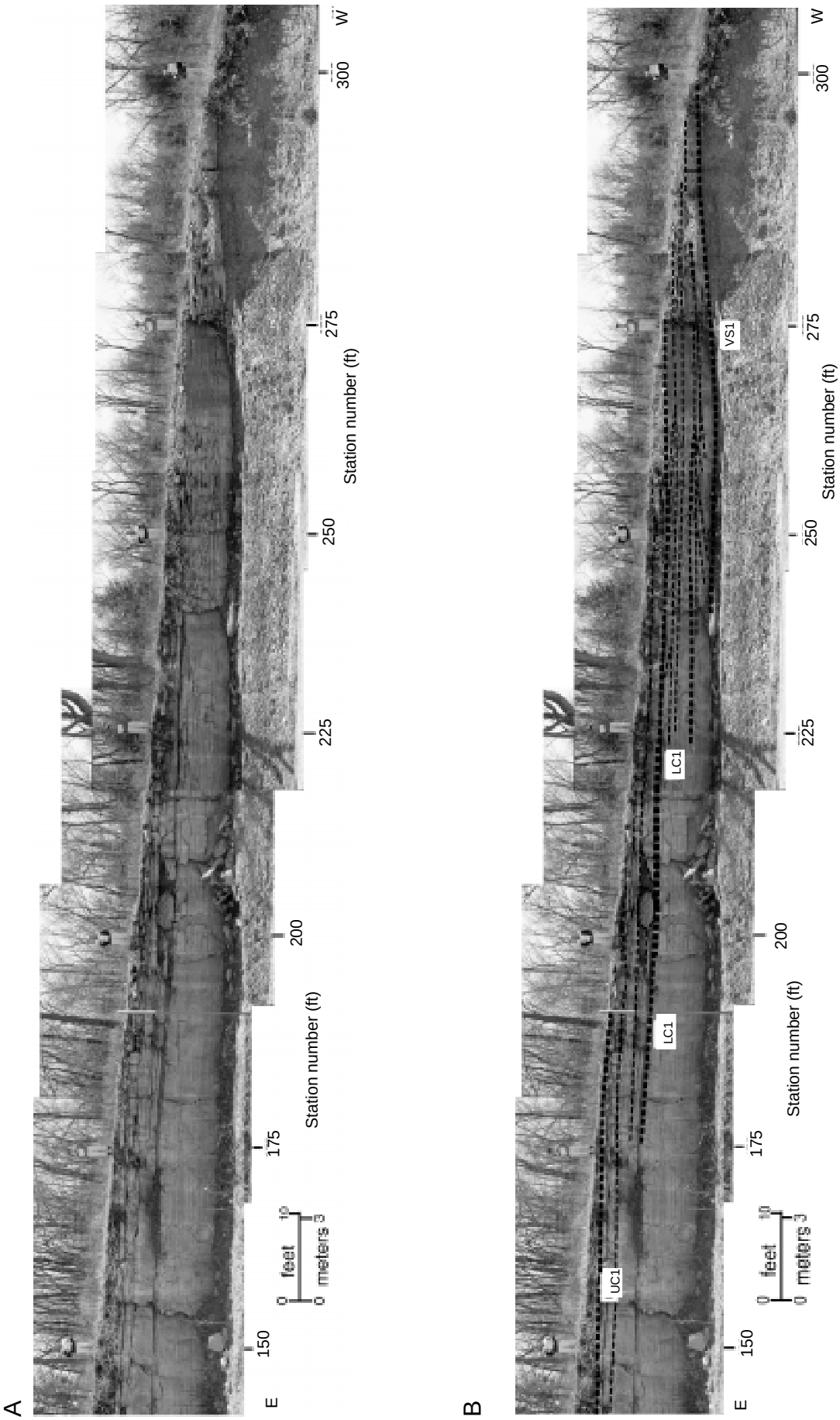


FIGURE 5. Uninterpreted (A) and interpreted (B) photomosaics from the Captain Creek study site. UC1, LC1, and VS1 refer to the upper Captain Creek Limestone Member, the lower Captain Creek Limestone Member, and the Vilas Shale, respectively. [Ed. note: A detailed view of this figure is available online at **www.kgs.ukans.edu/Current/1998/martinez/fig5.html.**]

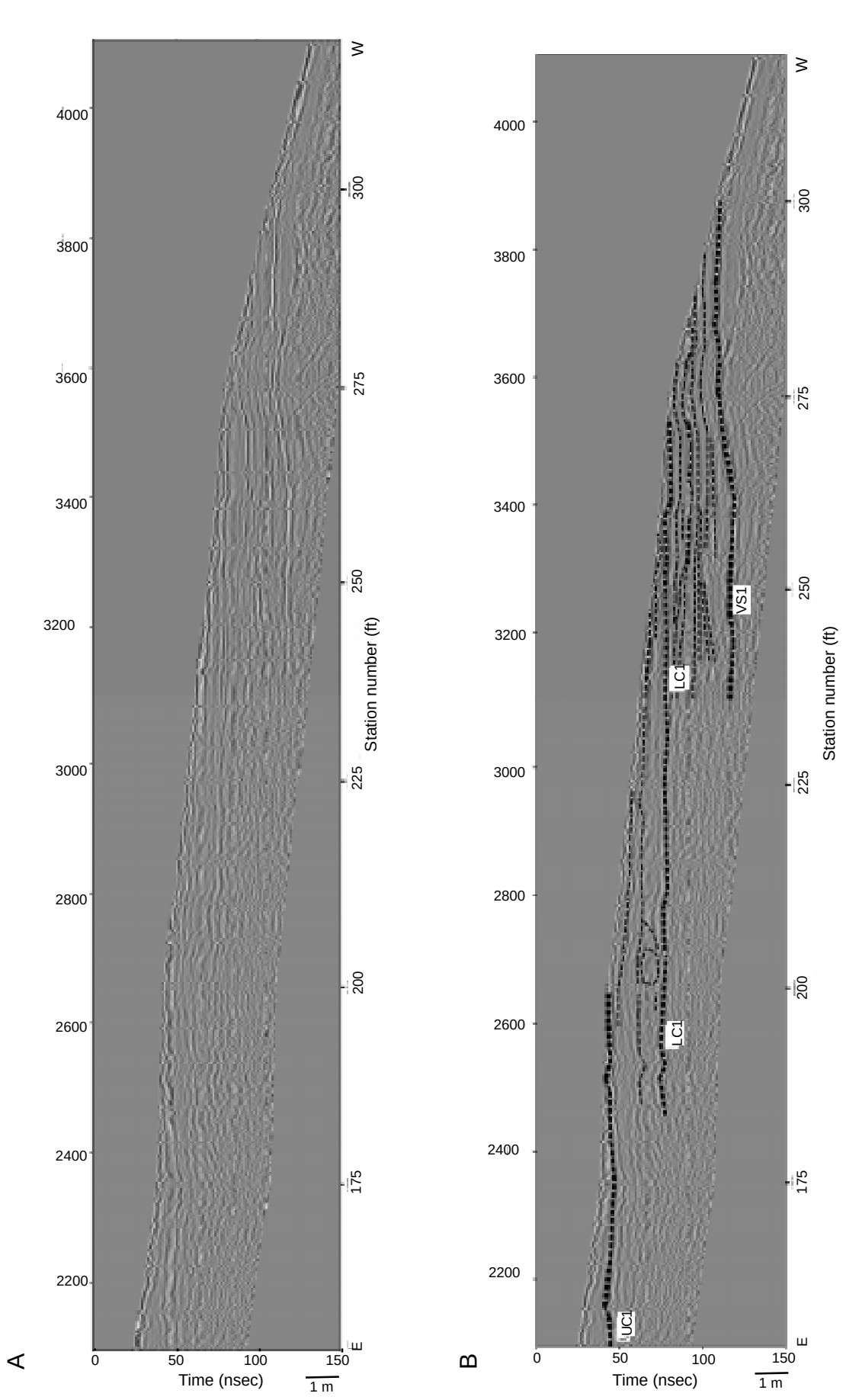


FIGURE 6. Uninterpreted (A) and interpreted (B) GPR profiles from the Captain Creek study site. Reflections seen on both GPR data and the outcrop are indicated by dashed lines. The GPR data have a vertical scale of two-way time in nanoseconds and a trace spacing of approximately 3 cm. UC1, LC1, and VS1 refer to the upper Captain Creek Limestone Member, the lower Captain Creek Limestone Member, and the Vilas Shale, respectively. [Ed. note: A detailed view of this figure is available online at **www.kgs.ukans.edu/Current/1998/martinez/fig6.html.**]

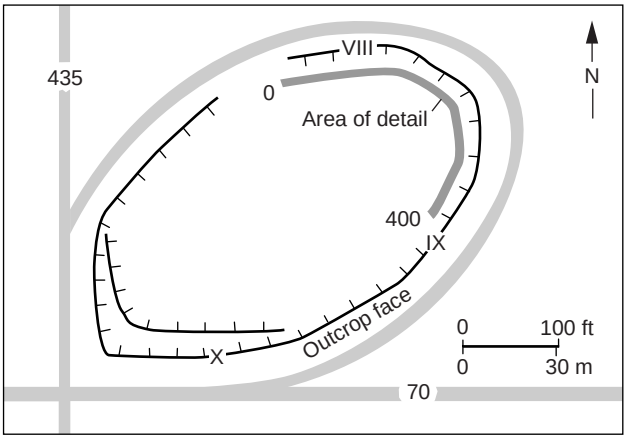


FIGURE 7. Map of the Plattsburg Limestone study site (see fig. 1 for location). The locations of the measured sections shown in fig. 8 are indicated by the roman numerals VIII, IX, and X. The location of the photomosaic and GPR profile shown in figs. 9 and 10 is indicated (area of detail).

from the contact between the Vilas Shale and the overlying lower Captain Creek Limestone Member near station 270 (fig. 6). This diffraction may have been due to a fracture or small fault responsible for the northward offset in the outcrop face near this station (fig. 5).

## Plattsburg Limestone

### Geologic setting

The Plattsburg Limestone study site is located in southwestern Wyandotte County, Kansas, on the northeastern access ramp of the interchange between I-435 and I-70 (figs. 1 and 7; stop 4 of Watney et al., 1989). GPR data were gathered at this site in order to image features associated with the Bonner Springs Shale (which caps the Wyandotte depositional sequence of Watney et al., 1989) and the Merriam Limestone Member of the Plattsburg Limestone (which forms the basal portion of the subjacent Plattsburg depositional sequence of Watney et al., 1989) (fig. 8). This site was chosen to determine the capabilities of GPR to image (1) hemi-channel forms within the sandstone lithology of the Bonner Springs Shale, (2) the erosional contact between the Merriam Limestone Member and Bonner Springs Shale, and (3) internal bedding geometries in the sandstone lithology of the Bonner Springs Shale and within the Merriam Limestone Member.

The Bonner Springs Shale outcrop at the study site consists of up to 8.7 m (28.5 ft) of channel sandstone overlain by 1.0 m (3.3 ft) of sandy shale, evidence of multiple episodes of erosional scouring and backfilling. The sandstone is extensively ripple cross-laminated, with a few festoon sets and local, climbing, ripple-drift cross lamination and herringbone crossbedding that is developed at the base (Enos et al., 1989). This sandstone, which apparently eroded the entire Bonner Springs Shale, is truncated by a distinct hemi-channel form (section X of fig. 8) filled with silty shale; silty, pebbly sandstone; and shale. The sand/shale hemi-channel form is truncated by another hemi-channel form expressed as abrupt westward thickening of the Merriam Limestone Member from 0.9 m in section IX to 4.0 m in section X of fig. 8.

The Merriam Limestone Member is the flooding unit of the Plattsburg sequence (Watney et al., 1989). Lithologically, the basal part is typically a packstone, but it ranges from very argillaceous, nodular-weathering yellow limestone to ooid grainstone. The middle portion of the bed, below the most prominent shale break, is typically a skeletal packstone containing prominent, coated grains or oncoids (Enos et al., 1989). An overlying shale bed or parting can be traced over most of the area. The top unit is one or two beds of skeletal packstone. Argillaceous limestone caps are developed locally.

### GPR interpretation and results

A site map of the study area shows the relationship between the GPR profile and the outcrop (fig. 7). Uninterpreted and interpreted photomosaics and GPR data from the site are shown in figs. 9 and 10. The data were plotted to 50 ns below the surface, corresponding to a depth of 3.0 m (9.8 ft), assuming an average one-way velocity of 0.12 m (0.39 ft)/ns (based on reflection traveltimes and unit thickness measured on the outcrop). Changes in relative elevation did not have an appreciable effect on limestone velocities, except when argillaceous units (which have slightly slower GPR velocity) were encountered at the surface.

Although data were collected along the entire 366-m (1,200-ft) pathway, only the data acquired between stations 0 and 400 (fig. 7) were visible. Based on outcrop observations, the lack of reflectivity in the remainder of the data was probably due to signal attenuation caused by a combination of thicker soil cover, conductive shale, a high content of conductive clays in the Bonner Springs sandstones and siltstones, and lack of significant dielectric-constant and lithologic contrasts in the underlying rock units. The boundaries between the major stratigraphic units were the locations of the most significant dielectric-constant contrasts. The internal contrasts were minor in comparison.

High-amplitude GPR reflections that were correlated with major unit boundaries on the outcrop are indicated by heavy dashed lines on figs. 9 and 10. These reflections divide the Merriam Limestone Member into five major reflective packages or units (ML1–ML5). Reflections within the major packages are identified by thin dashed lines (figs. 9 and 10) and were correlated with bedding planes visible on the outcrop. A transition from limestone to shaly limestone to limestone beds is observed in the Merriam member between stations 0 and 400 (fig. 9). This transition was also indicated by changes in the internal reflectivity of packages ML1–ML5 (fig. 10). Units ML1, ML2, and ML5 appear to represent the limestone beds,

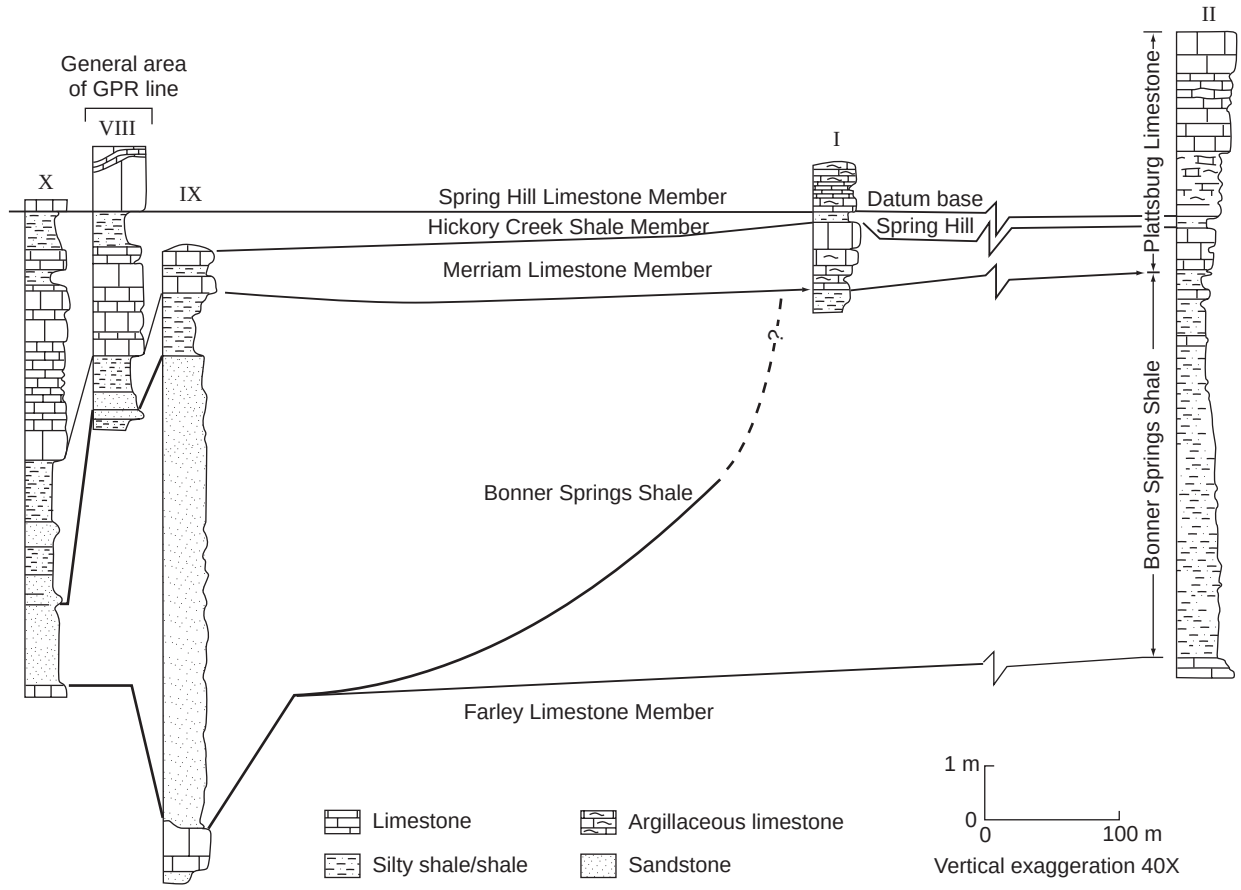


FIGURE 8. Measured stratigraphic sections and correlations of the Plattsburg Limestone (modified from Enos et al., 1989). The locations of measured sections VIII, IX, and X are shown on fig. 7.

while units ML 3 and ML4 represent shaly limestone beds (fig. 9). All of these units are generally flat-lying between stations 0 and 280 but were readily discernable from system noise on GPR data because they had slight variations in travel times and were not truly horizontal. The dips of beds increased between stations 280 and 400 as the margin of a series of hemi-channels was approached. This dip was mostly primary because the beds were deposited along the flanks of a channel. Primary dip was also indicated by flatter dips of overlying and underlying strata in some cases. However, the primary dip may have been partially exaggerated due to some compaction of underlying, finer-grained clastic units.

*Merriam Limestone Member (ML1).*—Unit ML1 is a distinct limestone bed directly beneath the modern land surface. The top of this bed was traceable between stations 120 and 265, whereas the base was imaged between stations 20 and 300 (figs. 9 and 10). Both the upper and lower contacts of this approximately 1.0-m (3.3-ft)-thick bed were imaged by GPR as relatively high amplitude reflections along most of its lateral extent. The large reflection amplitude of the top of ML1 might indicate that it is the contact between the Merriam Limestone Member and overlying Hickory Creek Shale Member. It is also possible that the reflection represents the base of a thicker soil layer, potentially a residual from the Hickory Creek. The low velocity of the overlying material was indicated by the slight velocity pull-down between stations 145 and 250 (fig. 10). Internal GPR reflections were of lower amplitude than those of stratigraphically lower limestone units. The reflection character of ML1 was likely due to its massive bedding and homogeneous limestone lithology, resulting in relatively small dielectric-constant contrasts internally.

*Merriam Limestone Member (ML2).*—Unit ML2 is a competent limestone that can be traced from stations 20 to 315 (fig. 9). Large-amplitude reflections within this unit (fig. 10) were probably due to argillaceous material between the limestone beds or compaction differences at bed boundaries. Gradual thickening and thinning of beds within unit ML2 was indicated on both the photomosaic (fig. 9) and the GPR data (fig. 10). The termination of the uppermost internal reflection near the top of unit ML2 between stations 220 and 230 (fig. 10) correlated with the thinning of a bed between this reflection and the top of ML2, which was consistent with outcrop observations. This reflection was characterized by a high-amplitude trough (white) with high-amplitude adjacent peaks (dark

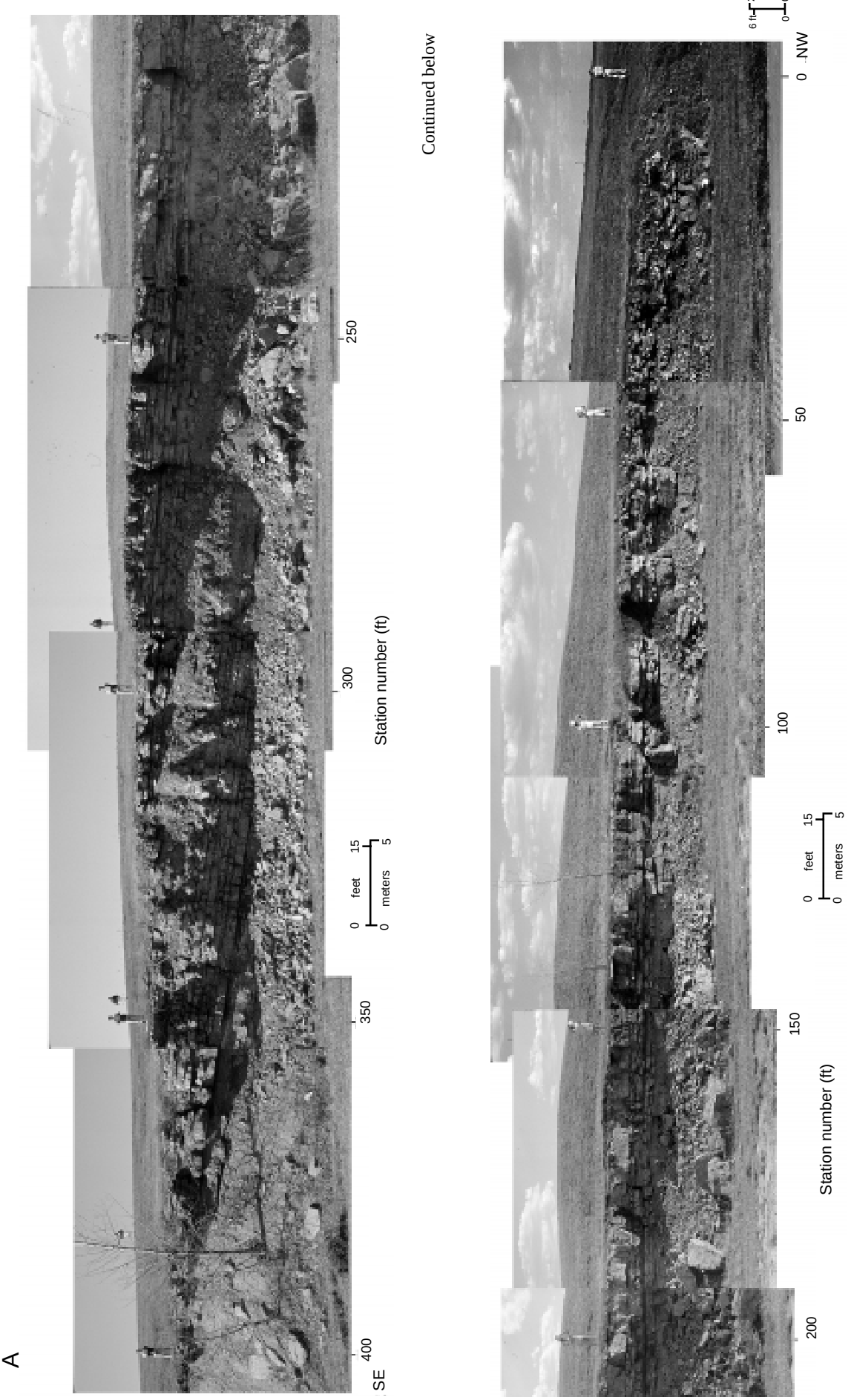


FIGURE 9A. Uninterpreted photomosaic from the Plattsburg Limestone study site. [Ed. note: A detailed view of this figure is available online at **www.kgs.ukans.edu/Current/1998/martinez/fig9.html.**]

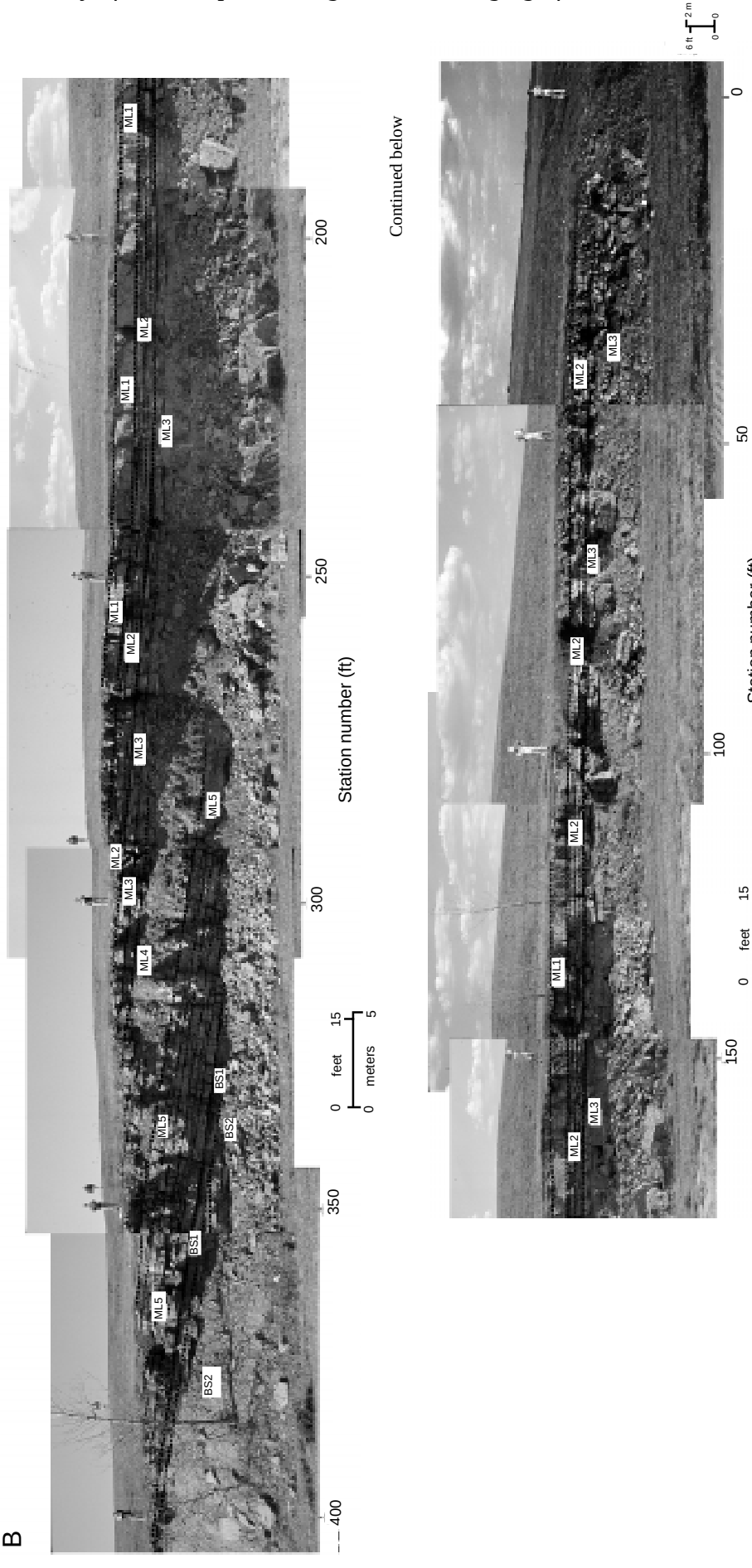


FIGURE 9B. Interpreted photomosaic from the Plattsburg Limestone study site. Reflections seen on both GPR data and the outcrop are indicated by dashed lines. ML1-6 and BS1-2 refer to bedding units within the Merriam Limestone Member and Bonner Springs Shale, respectively. [Ed. note: A detailed view of this figure is available online at **www.kgs.ukans.edu/Current/1998/martinez/fig9.html.**]

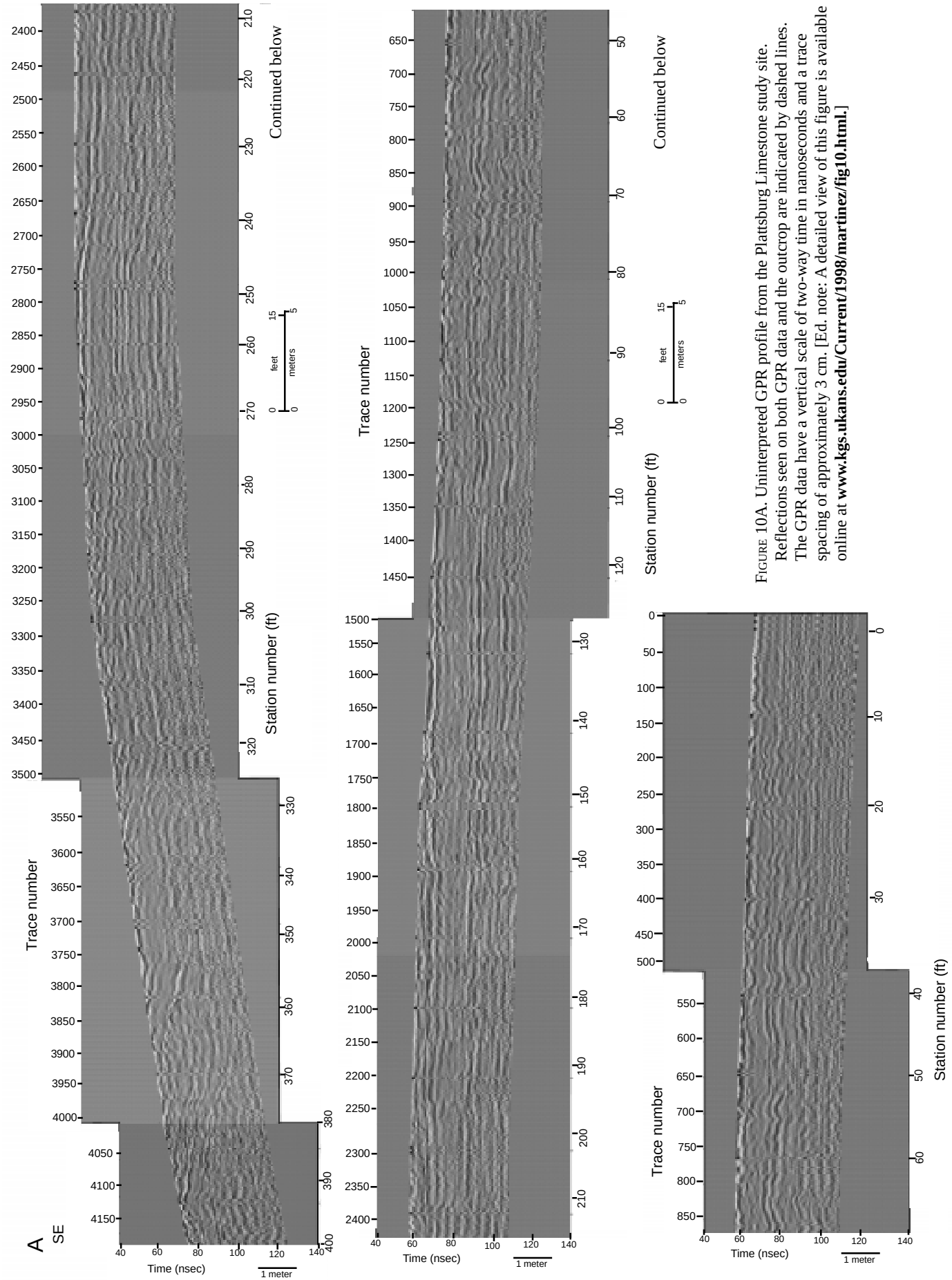


FIGURE 10A. Uninterpreted GPR profile from the Plattsburg Limestone study site. Reflections seen on both GPR data and the outcrop are indicated by dashed lines. The GPR data have a vertical scale of two-way time in nanoseconds and a trace spacing of approximately 3 cm. [Ed. note: A detailed view of this figure is available online at **www.kgs.ukans.edu/Current/1998/martinez/fig10.html.**]

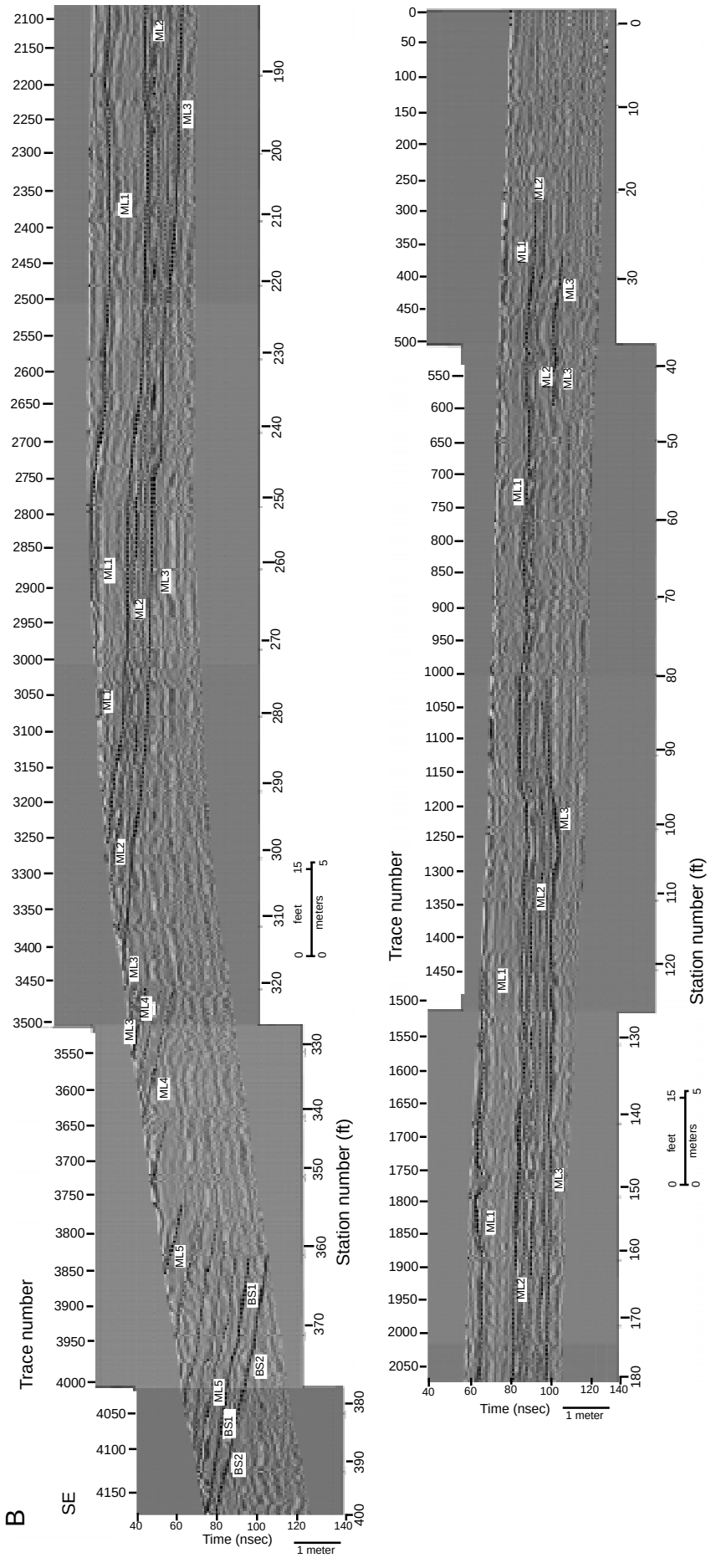


FIGURE 10B. Interpreted GPR profiles from the Plattsburg Limestone study site. Reflections seen on both GPR data and the outcrop are indicated by dashed lines. The GPR data have a vertical scale of two-way time in nanoseconds and a trace spacing of approximately 3 cm. ML1-6 and BS1-2 refer to bedding units within the Merriam Limestone Member and Bonner Springs Shale, respectively. [Ed. note: A detailed view of this figure is available online at **www.kgs.ukans.edu/Current/1998/martinez/fig10.html**.]

gray) along most of its length between stations 20 and 170. The relative strength of this reflection was gradually reduced between stations 170 and 190 due to a lessening of dielectric-constant contrasts. Beyond station 190 the reflection varied between a single event and a doublet as it interfered with the reflection associated with the top of ML2. This reflection ended between stations 220 and 230, as the bed became too thin to image with the 500-MHz GPR antenna.

*Merriam Limestone Member (ML3).*—The argillaceous limestone at the top of unit ML3 was well imaged between stations 30 and 315 (fig. 10), probably because of the large dielectric-constant contrast between it and the overlying lowermost limestone bed in unit ML2. The recessive weathering pattern of this unit suggests that it is predominantly a thin-bedded, shaly limestone that becomes more argillaceous downward (fig. 9). The high clay content of this unit may have caused the relatively low internal reflectivity and greater signal attenuation.

*Merriam Limestone Member (ML4).*—Unit ML4 is a shaly limestone that is more argillaceous and thinner bedded than unit ML3. Reflections from this unit were imaged only near the surface between stations 320 and 360. As in unit ML3, reflections from within unit ML4 were relatively weak, possibly due to high clay content at bounding surfaces and within the limestone unit, lack of significant internal dielectric-constant contrasts, and thin bedding. Diffractions from within unit ML4 occurred near the surface near station 340 (fig. 10). They may have been due to open fractures seen on the outcrop near the surface, the edges of collapse features, or modern weathering of this relatively easily erodable unit. The diffractions were not likely to have been caused by cobbles or out-of-plane reflections because of the GPR-profile distance from the outcrop face.

*Merriam Limestone Member (ML5).*—Unit ML5 is primarily a thin-to-medium-bedded limestone similar to unit ML2. It is relatively resistant and is visible in outcrop between stations 270 and 400 (fig. 9). This unit was imaged by GPR between stations 355 and 400 (fig. 10). The top of unit ML5 was a relatively strong reflection that was reduced in strength downdip due to signal attenuation caused by unit ML4. Internal reflections within unit ML5 were also attenuated by unit ML4. As with unit ML2, the high-amplitude reflectivity at bed boundaries was probably due to changes in clay content or compaction. Diffractions occurred along many of the bed boundaries in unit ML5 and were most apparent close to the surface at the top of the outcrop. As with the diffractions in unit ML2, they were probably caused by open or soil-filled joints and other fractures seen on the outcrop; they could possibly have been caused by the edges of modern collapse features seen in exposures at some locations. The base of this unit is an erosional contact between the Merriam Limestone Member and underlying Bonner Springs Shale. The interpretation of a hemi-channel form for the contact was supported by the westward thickening of the Merriam member visible on the outcrop (fig. 9), the GPR data (fig. 10), and measured stratigraphic sections (Enos et al., 1989) (fig. 8).

*Bonner Springs Shale (BS1).*—GPR successfully imaged the erosional contact (hemi-channel form) between the Bonner Springs silty shale lithology (BS1) and the overlying Merriam Limestone Member (ML5). The contact was visible on both the outcrop and GPR profile between stations 360 and 400, where measured section IX is located (fig. 8). The contact is expressed on the outcrop by low-angle truncation of dipping shale, silty shale, silty limestone, and siltstone layers in the Bonner Springs Shale (BS1) by the overlying Merriam Limestone Member (ML5). The Bonner Springs correlates with the distinct siltstone and shale-filled hemi-channel form below the Merriam member and above channel-filling sandstones and siltstones (measured sections VIII, IX, and X in fig. 8). This hemi-channel form was also supported by a very gradual thickening of unit BS1 downdip (fig. 9). The contact between the Bonner Springs Shale and Merriam Limestone Member is a relatively high amplitude reflection, but no more reflective than those between limestone beds in the overlying ML5 unit (fig. 10). Although the erosional truncation of beds is apparent on the outcrop, study of interference patterns did not show the termination of unit BS1 against the Merriam Limestone Member, probably because it was at too low an angle to image with the 500-MHz GPR antenna.

*Bonner Springs Shale (BS2).*—The top of unit BS2 is an erosional contact with a hemi-channel form that cuts across flatter-lying beds below (fig. 9). This unit correlates with the lower channel-filling sandstone and siltstone in measured sections VIII, IX, and X (fig. 8), which occur below the siltstone- and shale-filled hemi-channel form. The upper contact is obvious on the outcrop, but it was much less so on the GPR data. The relatively horizontal beds of siltstone, shaly siltstone, sandy siltstone, and sandstone are visible on the outcrop, but they were not imaged by GPR. The poor reflectivity along the top and within unit BS2 was probably due to signal attenuation caused by the siltstones in unit BS2, the silty to shaly layers in unit BS1, or a lack of significant dielectric-constant contrasts within the siltstones of BS2. The events seen at 80–100 ns between stations 390 and 400 were not related to beds within unit BS2, but instead were noise that appeared parallel to the ground surface.

## Discussion

High-frequency GPR can be an invaluable tool for enhancing outcrop studies because, with sufficient control, it allows detailed stratigraphic and lithologic information to be extended into the subsurface beyond the outcrop face in a relatively continuous manner. Detailed lateral and vertical stratigraphic and lithologic information is critical

to understanding the complex heterogeneity of reservoirs and can aid in determining production strategies. As our study shows, the shapes of bounding surfaces and channel fills can be imaged in the near surface via high-frequency GPR methods. In addition, our study indicates that vertical imaging resolutions of high-frequency GPR data are sufficient to image many small-scale details associated with these features, such as crossbedding and fractures. Imaging of channel fills and crossbedding can sometimes be used to determine stratal geometries in three dimensions, which can aid in determining paleoflow directions, which are important for establishing three-dimensional geometries of reservoir flow units (Beaty et al., 1997). GPR can be used to image subsurface features and extend outcrop correlations into areas of poor or nonexistent exposure, as long as there is a difference in dielectric constants between subsurface media and there is sufficient control on lithology and geometries from nearby outcrops or cores. The variability in GPR-amplitude responses is related to changes in the media through which the GPR signal passes, and therefore can sometimes be an indication of lithologic changes. Fine-grained material, such as clay and silt, can contain more bonded water molecules than coarser-grained material, thus increasing their dielectric constant if wet. Bounding surfaces between lithologic units may provide the largest dielectric-constant contrasts if they contain finer-grained siliciclastic material. In our study, bounding surfaces were enriched with fine-grained siliciclastics from both depositional and diagenetic processes. In contrast, internal dielectric contrasts within limestone units in our study usually are of lesser magnitude than those of major bounding surfaces because they usually contain thinner, less continuous siliciclastic layers. The massive-bedded and argillaceous units of the Plattsburg Limestone study site illustrate the utility of identifying reflection character and correlating it with subsurface lithology. At this site, the massive-bedded units have almost no internal reflections, whereas the argillaceous units have strong reflections from their upper bounding surfaces and cause significant signal attenuation.

This study was also successful in imaging joints and fractures at both study sites. The characteristics, diffractions, and offsets (sometimes accompanied by slight velocity pull-downs, when soil-filled) of these joints and fractures were confirmed using the data from the outcrop face. Therefore, by identifying reflection characteristics and correlating them to lithology and bedding features at the outcrop, general lithological and sedimentary structural information can be extended into the subsurface beyond the outcrop face. As noted by Knight et al. (1997), knowledge gained from GPR data of the shapes, spatial distribution, and frequency of these features (which may greatly affect reservoir quality) can help create more realistic reservoir models. As shown in the study by Martinez et al. (1998a), small-scale (less than 0.01 m; 0.03 ft) lithologic heterogeneity that affects permeability can be imaged using GPR methods. The results of that study, combined with those of the present study, indicate that laminae, beds, minor and major bounding surfaces, and fractures (all of which may affect fluid-flow characteristics within reservoir strata) can be imaged using GPR and thereby provide additional data for reservoir modeling efforts.

Previous outcrop studies involving GPR have usually used lower-frequency antennas and therefore have much lower vertical imaging resolutions (Pratt and Miall, 1993; Liner and Liner, 1995; Beres et al., 1995). Such resolution may be adequate for imaging relatively large-scale features (major bounding surfaces and faults), but it is not sufficient for imaging the detailed features (thin internal bedding and crossbedding) that were the concern of this study. It is also difficult to determine subtle lithological changes from lower-frequency data because the changes may occur at scales much smaller than the antenna wavelength.

Our study also differs from most previous studies in its detailed correlation of photomosaics of the outcrop face with reflection information. Detailed correlation of GPR data with the outcrop face is critical for understanding the cause of GPR reflections at a study site and recognizing subtle reflection characteristics of the data that allow interpretations to include small-scale lateral and vertical subsurface lithologic and stratigraphic variability.

The successful high-resolution imaging of major bounding surfaces, fractures, and joints indicates that high-frequency GPR may be a useful technique for mapping features associated with sequence-stratigraphic boundaries, including those evidencing paleokarst and paleosol development from subaerial exposure. Many important reservoirs, including those in the subsurface of Kansas, are associated with major sequence boundaries showing extensive subaerial exposure and karst features. GPR studies of analogs may provide an additional tool for quantifying the dimensions and spacing of fractures, caves, and joints associated with such sequence boundaries. Additionally, GPR may also aid in regional correlations of sequence boundaries. Using GPR for three-dimensional mapping of surfaces associated with sequence-stratigraphic boundaries can assist in placing outcrop information within a sequence-stratigraphic framework and help understand basin-scale depositional history, as well as provide important data for reservoir modeling.

Clearly, as shown by the various limiting factors at our study sites, high-frequency GPR is not a panacea for all outcrop studies. Not only is it limited to areas of low surface conductivity (e.g., those lacking clays or shales), it is also very limited in imaging depth because of rapid signal attenuation. For example, the 500-MHz GPR maximum-imaging depths in the limestone units of this study were approximately 3–4 m (9.8–13.1 ft). The penetration-depth limitations can be reduced by using a suite of antenna frequencies to image the subsurface at

different penetration depths and resolutions (Martinez et al., 1998b). Depth control of GPR data can also be a problem without adequate outcrop or borehole information to constrain possible GPR velocity values, even when using CDP gathers to determine velocity information. Having a detailed outcrop photomosaic to interpret alongside a GPR profile is critical if highly accurate, depth-constrained interpretations are necessary.

## Conclusions

Two petroleum-reservoir-analog outcrops of limestone units of interest were studied using high-frequency GPR methods to image stratigraphic architecture behind the outcrop face. GPR successfully imaged major bounding surfaces and features such as crossbedding and internal bedding within units in the subsurface to a maximum depth of 3–4 m (9.8–13.1 ft). Careful interpretation of the GPR data and correlation with outcrop information allowed general relationships between reflection characteristics and lithology to be determined. Strong reflections were found to correspond with major bounding surfaces, which consisted of either a decrease in grain size or change in lithology (often enriched with clay or siltstone), both of which resulted in a change in the electromagnetic properties of the rock at these locations.

At the Captain Creek study site, the contact between the Captain Creek Limestone Member and the Vilas Shale and the contact between the lower and upper units of the Captain Creek were successfully imaged using GPR methods. Additional internal features as small as 0.1–0.2 m (0.3–0.7 ft), such as soil-filled fractures and smaller-scale bedding units (including crossbedding within the lower and upper Captain Creek), were also imaged. Thick, clay-rich soil in the central portion of the outcrop greatly hampered GPR-signal penetration and limited the extent of GPR profiles.

At the Plattsburg Limestone study site, the erosional contact between the Bonner Springs Shale and the Merriam Limestone Member was successfully imaged using high-frequency GPR methods. Features as small as 0.1–0.2 m (0.3–0.7 ft), including smaller-scale bedding units and air- and soil-filled fractures within the Merriam Limestone Member, were also imaged. Identification of thinly bedded (less than 0.2 m; 0.7 ft), argillaceous intervals of the Merriam Limestone Member was possible because of the high resolution of 500-MHz GPR. However, signal penetration was reduced in the more argillaceous units of the Merriam member due to higher clay content. High-frequency GPR also had difficulty penetrating and imaging features within the Bonner Springs Shale because of rapid signal attenuation caused by the high conductivity of this unit. Lower-frequency GPR methods may provide more satisfactory results if used at this site to image features associated with the Bonner Springs Shale.

Overall, GPR was successful in imaging detailed stratigraphic architectural elements as small as 0.1–0.2 m (0.3–0.7 ft) at each study site. Detailed correlation between GPR and outcrop data allows the use of pattern recognition when away from outcrops or boreholes. With a nearby outcrop, the shapes and patterns of sedimentary features can be recognized and then extrapolated into the subsurface with some confidence. Further GPR imaging of these reservoir analogs could provide information about three-dimensional changes in stratigraphy and lithology that may be useful in exploitation of valuable petroleum resources.

## Acknowledgments

The authors wish to thank Neil Anderson, Mike Roark, and Mike Shoemaker of the University of Missouri–Rolla, for the use of UMR's radar equipment and field assistance in this study. David Leck provided field assistance at the Plattsburg Limestone study site, and Rich Sleezer performed soil sample analyses for the Captain Creek study site. Critical reviews by Rick Miller, Toni Simo, and Roger Young greatly aided us in clarifying our ideas and strengthening the paper, and editing by Liz Brosius helped make the paper more accessible. Lastly, Tim Carr of the Kansas Geological Survey graciously provided funding for this study.

## References

Beaty, D. S., Martinez, A., and Walton, A. W., 1997, Combined minipermeameter and ground-penetrating radar characterization of valley-fill sandstones, Upper Pennsylvanian, northeastern Kansas: Proceedings of the Gulf Coast Section of the 1997 SEPM Annual Conference, p. 41–54.

Beres, M., Green, A., Huggenberger, P., and Horstmeyer, H., 1995, Mapping the architecture of glaciofluvial sediments with three-dimensional georadar: Geology, v. 23, no. 12, p. 1,087–1,090.

Bridge, J. S., Alexander, J., Collier, R. E., Gawthorpe, R. L., and Jarvis, J., 1995, Ground-penetrating radar and coring used to study the large-scale structure of point-bar deposits in three dimensions: Sedimentology, v. 42, p. 839–852.

Brown, H. A., 1963, Examination of Pennsylvanian carbonate banks in southwestern Kansas: Kansas Geological Survey, Open-file Report 63-5, 9 p.

Cunningham, K. J., and Franseen, E. K., 1992, Conglomeratic limestones of the Upper Pennsylvanian Captain Creek Limestone and their association with the lower sequence boundary of the Stanton depositional sequence, Northwestern Johnson County, Kansas: Kansas Geological Survey, Open-file Report 92-51, 47 p.

Daniels, D. J., 1996. Surface-penetrating radar; *in*, IEEE Radar, Sonar, Navigation and Avionics Series 6, E. D. R. Sharman and P. Bradsell, eds.: Exeter, United Kingdom, Short Run Press Ltd., 300 p.

Davis, J. L., and Annan, A. P., 1989, Ground-penetrating radar for high-resolution mapping of soil and rock stratigraphy: Geophysical Prospecting, v. 37, p. 531–551.

Dominic, D. F., Egan, K., Carney, C., Wolfe, P. J., and Boardman, M. R., 1995, Delineation of shallow stratigraphy using ground-penetrating radar: Journal of Applied Geophysics, v. 33, p. 167–175.

Enos, P., Herman, D., Watney, W. L., and Franseen, E., 1989, Stop 4 I-70/I-435 interchange—Bonner Springs Shale and Plattsburg Limestone; *in*, Sequence Stratigraphic Interpretations and Modeling of Cyclothems in the Upper Pennsylvanian (Missourian), Lansing and Kansas City Groups in Eastern Kansas: Kansas Geological Society Guidebook, 41st Annual Field Trip, October 14–15, 1989, Kansas Geological Survey, Open-file Report 89-44, p. 115–126.

Feldman, H. R., and Franseen, E. K., 1991, Stratigraphy and Depositional History of the Drum Limestone and Associated Strata (Pennsylvanian) in the Independence, Kansas, Area-A Field Trip Guidebook and Road Log: Kansas Geological Survey, Open-file Report 91-45, 29 p.

Franseen, E. K., Feldman, H. R., Anderson, N. L., and Miller, R. D., 1995, Depositional and stratigraphic analysis of Kansas City group strata utilizing high-resolution seismic imaging, Montgomery County, Kansas; *in*, Geophysical Atlas of Selected Oil and Gas Fields in Kansas, N. L. Anderson and D. E. Hedke, eds.: Kansas Geological Survey, Bulletin 237, p. 43-46.

Gawthorpe, R. L., Collier, R. E., Alexander, J., Bridge, J. S., and Leeder, M. R., 1993, Ground-penetrating radar—Application to sandbody geometry and heterogeneity studies: Geological Society, Special Publication no. 73, p. 421–432.

Hamblin, W. K., 1969, Marine paleocurrent directions in limestones of the Kansas City Group (Upper Pennsylvanian) in eastern Kansas: Kansas Geological Survey, Bulletin 194, pt. 2, 25 p.

Jol, H. M., Smith, D. G., Meyers, R. A., and Lawton, D. C., 1996, Ground penetrating radar—High resolution stratigraphic analysis of coastal and fluvial environments: Gulf Coast Section of the SEPM Foundation 17th Annual Research Conference on Stratigraphic Analysis, p. 153–163.

Knight, R., Tercier, P., and Jol, H., 1997, The role of ground-penetrating radar and geostatistics in reservoir description: The Leading Edge, v. 16, no. 11, p. 1,576–1,582.

Kruger, J. M., Martinez, A., and Franseen, E. K., 1996, A high-frequency ground-penetrating radar study of the Drum Limestone, Montgomery County, Kansas: Kansas Geological Survey Open-file Report 96-49, 17 p.

Liner, C. L., and Liner, J. L., 1995, Ground penetrating radar—A near-face experience from Washington County, Arkansas: The Leading Edge, v. 14, no. 1, p. 17–21.

Martinez, A., Kruger, J. M., Franseen, E. K., Shoemaker, M. L., and Roark, M. L., 1995a, A high-frequency ground-penetrating radar study of the Captain Creek Limestone, Johnson County, Kansas: Kansas Geological Survey, Open-file Report 95-57, 23 p.

Martinez, A., Kruger, J. M., and Franseen, E. K., 1995b, A high-frequency ground-penetrating radar study of the Plattsburg Limestone and Bonner Springs Shale, I-435/I-70 Interchange, Southwest Wyandotte County, Kansas: Kansas Geological Survey, Open-file Report 95-58, 52 p.

Martinez, A., Feldman, H. R., Kruger, J. M., and Beaty, D. S., 1996, Three-dimensional characterization of a fluvial sandstone reservoir analog in northeast Kansas using high-resolution ground-penetrating radar: Kansas Geological Survey, Open-file Report 96-38, 30 p.

Martinez, A., Beaty, D. S., Stiles, J., and Carr, T. R., 1998a, Comparison of ground-penetrating radar reflectivity and rock properties in a sandstone-dominated incised valley-fill deposit: Proceedings Volume 2, Seventh International Conference on Ground Penetrating Radar, University of Kansas, Lawrence, KS, p. 693–698.

Martinez, A., Franseen, E. K., and Beaty, D. S., 1998b, Applications of ground-penetrating radar to sedimentologic and stratigraphic studies—Examples from Pennsylvanian silciclastics and carbonates in Kansas: Proceedings Volume 2, Seventh International Conference on Ground Penetrating Radar, University of Kansas, Lawrence, KS, p. 687–692.

Miller, R. A., Anderson, N. L., Feldman, H. R., and Franseen, E. K., 1995, Vertical resolution of a seismic survey in carbonate and siliciclastic sequences less than 100 m deep in southeastern Kansas: Geophysics, v. 60, p. 423–430.

Newell, K. D., Watney, W. L., Cheng, S. W. L., and Brownrigg, R. L., 1987, Stratigraphic and spatial distribution of oil and gas production in Kansas: Kansas Geological Survey, Subsurface Geology Series 9, 86 p.

Pratt, B. R., and Miall, A. D., 1993, Anatomy of a bioclastic grainstone megashoal (Middle Silurian, southern Ontario) revealed by ground-penetrating radar: Geology, v. 21, no. 3, p. 223–226.

Schon, J. H., 1996, Physical Properties of Rocks: Fundamentals and Principles of Petrophysics: Tarrytown, New York, Elsevier Science Inc., p. 465–478.

Watney, W. L., 1980, Cyclic sedimentation of the Lansing and Kansas City groups (Missourian) in northwestern Kansas and southwestern Nebraska—A guide for petroleum exploration: Kansas Geological Survey, Bulletin 220, 72 p.

Watney, W. L., French, J. A., and Franseen, E. K., eds., 1989, Sequence stratigraphic interpretations and modeling of cyclothems in the Upper Pennsylvanian (Missourian), Lansing and Kansas City Groups in eastern Kansas: Kansas Geological Society Guidebook, 41st Annual Field Trip, October 14–15, 1989, Kansas Geological Survey, Open-file Report 89-44, 211 p.